Modeling of Spatially Periodic Dielectric Sensors in the Presence of a Top Ground Plane Bounding the Test Dielectric

Y. Sheiretov
JENTEK Sensors, Inc.
Waltham, 110-1 Clematis Ave., MA, 02451-7013, USA

M. Zahn
Massachusetts Institute of Technology
77 Massachusetts Avenue, Cambridge, MA, 02139, USA

ABSTRACT

Semi-analytical models are used to simulate the response of periodic-field electroquasistatic dielectrometry sensors. Due to the periodic structure of the sensors it is possible to use Fourier series methods in combination with collocation point numerical techniques to generate accurate sensor simulations much more efficiently than with the more general finite-element methods. Previously, collocation-point models used to compute the response of periodic field dielectric sensors, also known as Interdigitated Electrode Dielectrometers (IDED), have ignored the contribution of the constant (zero-order) term in the Fourier series expansion of the physical quantities. This is justifiable if the top dielectric material layer under test is infinitely thick, with any top ground plane bounding the dielectric removed too far from the sensor to influence its response. This is the assumption generally made until now in the application of these models. In practice, however, it is impossible to eliminate the cumulative effect of objects at ground potential in the vicinity of the sensor, which in general manifests itself as a ground plane electrode positioned at some effective distance within the top dielectric layer (usually air). In order to eliminate this source of uncertainty in the measurements, we suggest that a grounded electrode be explicitly placed at the top of the dielectric layer in the experimental setup, and its presence be accounted for in the models. Furthermore, in many cases, such as measurements on ceramic thermal barrier coatings, a metal layer is already present behind the material under test.

In this paper we present how the models must be modified to account for this ground plane, and what effect it has on the dependence of the sensor response on the material properties. For example, the sensor transcapacitance may no longer be a monotonically increasing function of the material's permittivity, leading to non-uniqueness in permittivity measurements, as some field lines will terminate at the top ground plane rather than on the sensing electrode. We present experimental data that confirm these models.

1 INTRODUCTION

The basic idea behind periodic field electroquasistatic dielectrometers is that the electrodes are laid out in a spatially periodic pattern on a substrate, making one-sided contact with the dielectric material under test. The imposed spatial period (wavelength) λ determines the rate of decay of the fields away from the sensor and is chosen to achieve the desired depth of sensitivity. The frequency of excitation does not affect this depth of sensitivity for low loss dielectrics. The periodic nature of the potentials and fields allows for the use of Fourier series methods in the semi-analytical models.

The spatially periodic quasistatic sensors have several advantages over alternative sensing technologies:

- Control over the depth of sensitivity allows for measuring profiles of material properties by combining the results of measurements at varying depths, controlled by varying sensor wavelength.
- The layout allows for a good match between simulated and measured sensor response with the simulations carried out with efficient collocation point methods.

Manuscript received on 26 March 2005, in final form 21 July 2005.

This reduces the need for elaborate calibration standards and procedures.

- The flexible substrate makes it possible to measure on curved surfaces, with the curvature having no appreciable effect on sensor response.
- The sensor geometry allows for the creation of sensor arrays, to allow scanning over large areas with good uniformity between individual array elements. The simulation methods remain valid for arrays.
- The Fourier series analysis together with collocation point numerical techniques offers greater insight on the effects of material dielectric and conduction properties, layer thicknesses, and frequency and is usually much faster and more accurate than finite element methods. The semi-analytical Fourier series analysis is often used to precompute the solutions for graphical display or in look-up tables so that measurements can be easily compared to theory. This analysis is typically done for wide ranges of material dielectric and conduction properties and layer thicknesses by simply changing one property at a time and using the precomputed results to quickly obtain the answer. Performing the same number of case studies using the finite-element method one at a time, would be much more time consuming.

The layout of a typical interdigitated dielectrometer is shown in Figure 1. A voltage V_D is applied to the driven electrode, whereas the sensing and guard electrodes are kept at ground potential. A spatially periodic electric field is generated, which penetrates the material under test. The electric field lines originate on the driven electrode and terminate on the sensing or guard electrodes. The sum of the changing displacement and conduction currents to the sensing electrode are equal to the terminal current I_S. The sensor's complex transadmittance, defined as $Y_{21} = I_S/V_D$, is directly linked to the dielectric, conduction, and geometric properties of the material under test.

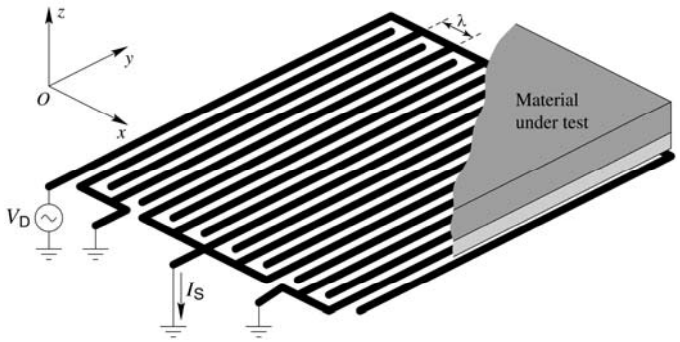

Figure 1. Schematic layout of an IDED. There are two interdigitated comb electrodes. A driving voltage V_D is applied to one of them, the driven electrode, whereas the second one, the sensing electrode, is kept at ground potential. The sensor transadmittance, which is the quantity measured by the impedance analyzer, is defined as $Y_{21} = I_S/V_D$, where I_S is the current out of the sensing electrode. Two grounded fingers at either side do not contribute to the signal I_S in order to reduce the end effects due to the sensor's finite width in the x-direction.

The sensor electrodes are laid out on a dielectric substrate. A side view of the interdigitated dielectrometer in contact with a material structure that consists of several layers of homogeneous dielectric materials is shown in Figure 2. On the side opposite to the sensor electrodes the substrate is bounded from below by a metal plane electrode kept at ground potential, hereafter referred to as the "substrate ground plane." The dielectric material structure under test can either be bounded at the top by another grounded plane electrode, referred to as the "top ground plane," or it can have a top layer, typically air, that extends to infinity, *i.e.*, its top surface is too far from the sensor to influence its response. The former case is more general, because the latter can be treated as a special case by setting the thickness of the top layer t_4 in Figure 2 to infinity.

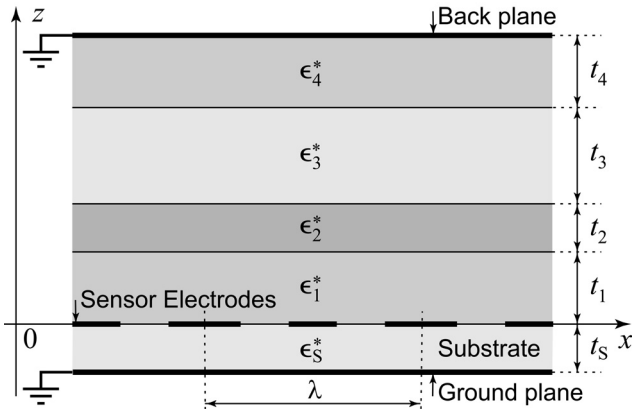

Figure 2. Side view of the IDED, in contact with a material structure that consists of several layers of homogeneous, lossy dielectric materials with complex permittivity ε^*, defined in equation (10).

In the case of an infinitely thick top layer, far from the sensor the electric field assumes the form of a dipole field, because the substrate ground plane is at zero potential, whereas in the plane of the electrodes the potential has a nonzero average value. This makes the sensor somewhat susceptible to the presence of other objects in the vicinity, thus compromising measurement repeatability. With a top ground plane, however, the electric field is entirely contained within the sensor structure.

The Interdigitated Electrode Dielectrometer (IDED*) is suitable for measurements on insulating or slightly conducting dielectric materials. It is in use in several practical applications:

- Cure monitoring of polymers, epoxy, etc. [1].
- Measurement of porosity and thermal conductivity in ceramic thermal barrier coatings [2].
- Moisture measurement in transformer oil and pressboard [3–5].
- Thin film characterization.

The cure monitoring application has received some attention recently [1]. During the chemical reactions of the curing process the materials exhibit significant conductivity, which is a strong function of the curing stage and continues to

* IDED is a trademark of JENTEK Sensors, Inc.

decrease for a long time after the compound has officially attained its full strength. The conductivity is due to the presence of free radicals during curing. Its value and rate of change are directly related to the curing process, making it possible to identify clearly the different stages of the chemical reaction. Furthermore, from the point of view of the parameter estimation methods, the presence of conductivity adds another degree of freedom in the form of nonzero imaginary transcapacitance component. The measurement of moisture in dielectrics also takes advantage of the presence of finite conductivity in the insulation.

The depth of sensitivity of the sensor depends on the imposed spatial wavelength. Combining the results of sensors with different wavelengths can be used to measure properties as a function of depth or to estimate more than one unknown parameter. This is especially useful for measurements where direct contact with the material is not possible, such as noncontact cure monitoring [1]. The lift-off, *i.e.*, the air gap thickness, is usually not known, especially with the material deposited on a moving web, where some vertical motion, or flutter, is inevitable. This requires the simultaneous estimation of three unknown parameters: the permittivity and conductivity, which change with cure state, and the lift-off. What complicates matters even more is that the thickness of the film may be nonuniform, adding another unknown to the set of properties that need to be simultaneously estimated.

In cases like this it is beneficial to combine the response of several sensors with different spatial periods. Multiple-wavelength dielectrometers have also been used to monitor the diffusion of moisture into pressboard. The moisture content is related to the conductivity and permittivity. The use of multiple wavelength sensors makes it possible to measure the variation of the conductivity and permittivity with depth [4, 5].

Cartesian geometry interdigital electrode dielectrometry (IDED) sensors assume that: (1) the extent of the sensor is infinite in the y-direction with all physical quantities independent of y; and (2) the sensor extends to infinity in the x-direction and all physical quantities are spatially periodic in the x-direction with a wavelength λ [3, 6].

The periodic structure of the IDED makes it possible to represent the electrostatic potential Φ, as a Fourier series with a fundamental wavenumber $k = 2\pi/\lambda$. The sensing electrode is kept at virtual ground potential via a feedback circuit. The value of the electrostatic potential is thus known at both electrodes, being equal to the driving voltage V_D at the driven electrode, and zero at the sensing electrode. In the gap between the electrodes it is determined via a collocation point method, as discussed in the next section.

Regardless of the exact details of the model, for each Fourier mode (including the zero-order mode), the effect of the material under test may be expressed in terms of the value of the surface capacitance density, defined in Section 2.3, at the plane of the electrodes ($z = 0$). The focus of this paper is the proper derivation of this quantity in the presence of a grounded top plane bounding the dielectric material under test. As part of this analysis, it is demonstrated that the constant (zero-order) term in the Fourier Series expansion may not be neglected, as was done in earlier work [3].

2 MODELING

In the most common configuration, a measurement with an electroquasistatic dielectrometer is carried out with an impedance analyzer. The quantity being measured is the sensor transadmittance, defined as $Y_{21} = I_S/V_D$, where V_D is the complex magnitude of the voltage applied at one of the electrodes (the driven electrode) and I_S is the complex magnitude of the current that flows out of the other electrode (the sensing electrode), which is kept at ground potential. In the Cartesian geometry sensors the two electrodes form an interdigitated comb pattern, as shown in Figure 1**,** and are geometrically equivalent.

The goal of this method is to compute the sensor transadmittance from the dielectric and geometric properties of the material under test and the geometric and dielectric properties of the sensor.

2.1 COLLOCATION POINT METHOD

This method approximates the unknown potential in the gap between the two interdigitated electrodes as an interpolation between its values, v_m, at a set of points in the gap, called the collocation points. The values v_m are computed by solving a set of simultaneous equations, each of which is derived from a boundary condition applied over a spatial interval that contains the point x_m.

The collocation point method takes the following steps to compute the sensor transcapacitance from its geometry and the properties of the material under test:

1. Solve Laplace's equation to determine the functional form of the electrostatic potential and the electric field intensity.
2. Express the potential in the plane of the sensor by its values (to be determined) at a set of collocation points and a suitable interpolation function.
3. Represent the potential as a Fourier series. Derive the series coefficients in terms of the potential values at the collocation points.
4. For each Fourier mode, compute the surface capacitance density, which relates the electric field intensity to the electrostatic potential, from the properties of the material under test.
5. Apply boundary conditions over a set of spatial intervals containing the collocation points to obtain constraining equations. Solve the resulting linear system of equations.
6. Use the thus obtained potential to compute the electric fields and integrate them over the sensing electrode area to compute the electrode terminal current I_S.

2.2 LAPLACE'S EQUATION

For the purpose of this model it is assumed that the sensor is infinite and uniform in the y-direction. Due to the spatial periodicity in the x-direction, the useful set of solutions to Laplace's equation $\nabla^2\Phi = 0$ are

$$\Phi(x,z) = \left[a_1 \sin(kx) + a_2 \cos(kx)\right]\left(b_1 e^{kz} + b_2 e^{-kz}\right) + \left(c_1 + c_2 x\right)\left(d_1 + d_2 z\right) \quad (1)$$

The zero reference of the electric scalar potential is fixed by the presence of grounded electrodes (top and substrate ground planes). As a consequence, in the plane of the electrodes the potential can have a nonzero component constant with x, requiring the consideration of the last term in equation (1).

If the $x = 0$ point is chosen at the middle of a drive electrode, the even symmetry dictates that $a_1 = 0$ and $c_2 = 0$ in equation (1), and without loss of generality $a_2 = 1$ and $c_1 = 1$. The remaining relevant solutions are

$$\Phi(x,z) = \cos(kx)\left(b_1 e^{kz} + b_2 e^{-kz}\right) + d_1 + d_2 z \quad (2)$$

The electric field corresponding to the potential in equation (2) is given by:

$$\mathbf{E} = -\nabla\Phi = k\sin(kx)\left(b_1 e^{kz} + b_2 e^{-kz}\right)\hat{\mathbf{x}} - \left[k\cos(kx)\left(b_1 e^{kz} - b_2 e^{-kz}\right) + d_2\right]\hat{\mathbf{z}} \quad (3)$$

Equation (2) implies that the scalar potential may be represented as a Fourier cosine series, because, due to the periodic structure of the sensor, all physical quantities are periodic with period λ:

$$\Phi(x,z) = \Phi_0(z) + \sum_{n=1}^{\infty} \Phi_n(z)\cos(k_n x), \qquad k_n = \frac{2\pi n}{\lambda} \quad (4)$$

The expansion includes a zero-order term $\Phi_0(z)$, since the reference point of the potential cannot be chosen arbitrarily, having already been determined by the ground potential at the sensing electrode and the two ground planes. The series coefficients $\Phi_n(z)$ are related to the continuous potential via the following equations [7]:

$$\Phi_n(z) = \frac{4}{\lambda}\int_0^{\lambda/2} \Phi(x,z)\cos(k_n x)\,dx \quad (5)$$

$$\Phi_0(z) = \frac{2}{\lambda}\int_0^{\lambda/2} \Phi(x,z)\,dx \quad (6)$$

2.3 SURFACE CAPACITANCE DENSITY

There are two parameters of a medium that determine the quasistatic distribution of electric fields: the dielectric permittivity ε and the conductivity σ. The former determines the displacement current density from the electric field, whereas the latter relates the conduction current density to the electric field. The permittivity governs energy storage (reactive power) phenomena, whereas the conductivity determines the power dissipation (active power). It is possible to combine these two effects by adding the effect of the ohmic conductivity to the imaginary (loss) component of the complex permittivity.

Consider an electrode in contact with a medium as shown in Figure 3. In the one-dimensional geometry in the figure, the current density and the electric field are perpendicular to the electrode. Let the normal component of the electric field at the electrode surface be **E**. The terminal current I can be obtained by integrating the total current per unit electrode area **J** that flows into the electrode. The total current density is given by

$$\mathbf{J} = \mathbf{J}_C + \mathbf{J}_D = \sigma\mathbf{E} + \frac{d}{dt}(\varepsilon\mathbf{E}) \quad (7)$$

where $\mathbf{J}_C$ is the conduction current density and $\mathbf{J}_D$ is the displacement current density.

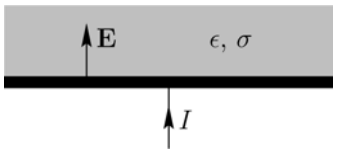

Figure 3. Terminal current of an electrode in contact with a conducting dielectric medium.

Under sinusoidal steady state operation at angular frequency ω all time dependent variables can be written in the form

$$\mathrm{F}(t) = \Re e\left\{F e^{i\omega t}\right\} \quad (8)$$

where F is the complex amplitude, equation (7) can be expressed in terms of complex amplitudes as

$$J = J_C + J_D = \sigma E + i\omega\varepsilon E = i\omega E\left(\varepsilon + \frac{\sigma}{i\omega}\right) \quad (9)$$

where $i = \sqrt{-1}$. We assume that the dielectric is nondispersive, *i.e.,* ε^* is not a function of frequency. This assumption is justified because for frequencies below 100 kHz, at which the sensors are operated, all dielectric materials on which these sensors are used, *e.g.*, plastics, ceramics, etc., show negligible dispersion. It is possible to include conduction loss to analyses that otherwise consider only insulating dielectrics simply by replacing ε in a medium with the corresponding *complex permittivity* ε^*, defined as:

$$\varepsilon^* = \varepsilon' - i\varepsilon'' = \varepsilon - i\frac{\sigma}{\omega} \quad (10)$$

This makes it possible to rewrite equation (9) as

$$J = i\omega\varepsilon^* E \quad (11)$$

For a particular spatial Fourier mode n, many quantities have the same $\cos(k_n x)$ dependence on x. It is therefore convenient to adopt the following notation, assigning the function name with a tilde (~) accent to account for the z-dependence of any quantity F:

$$F_n(x,z) = \tilde{F}_n(z)\cos(k_n x) \quad (12)$$

Using $\mathbf{E} = -\nabla\Phi$, the normal electric field intensity can be expressed in terms of the potential as $E_{z,n}(x,z) = -\frac{\partial}{\partial z}\Phi_n(x,z)$, which, using this notation, can be written in abbreviated form as

$$\tilde{E}_{z,n}(z) = -\frac{d}{dz}\tilde{\Phi}_n(z) \tag{13}$$

Consider a material structure with several homogeneous layers, as shown in Figure 2. The top layer borders on the top ground plane electrode. This is a good model even if no such electrode is present in an experimental setup, since there are many objects in the vicinity which are at ground potential, which act as a ground at a certain effective distance [6]. In fact, it is better to explicitly place a grounded metal plate behind the material under test, so that it is at a controlled distance to be used in the model. Nonetheless, it is still possible to model a structure with no top ground plane by letting the thickness of the top layer approach infinity. Both cases are treated in this paper.

In the electroquasistatic regime, it is possible to define the *complex surface capacitance density* as

$$C_n^*(z) = \frac{\varepsilon^*(z)\tilde{E}_{z,n}(z)}{\tilde{\Phi}_n(z)}, \qquad n = 0,1,2,\ldots \tag{14}$$

In terms of its effect on the sensor transcapacitance, all information about the material under test is contained in the value of $C_n^*(z)$ at $z = 0$ for all spatial Fourier modes. Note that $\varepsilon^*(z)\tilde{E}_{z,n}(z)$, $\tilde{\Phi}_n(z)$, and therefore $C_n^*(z)$, are continuous in the z-direction at material interfaces with no electrodes.

The goal is to compute C_n^* at the electrode position (at $z = 0$). First consider a homogeneous material layer (*i.e.*, ε^* is constant) that extends to infinity in the positive z-direction, with bottom interface at $z = z_0$. Out of the solutions in equation (2), only the e^{-kz} term remains finite at $z = \infty$, leading to

$$\tilde{\Phi}_n(z) = \tilde{\Phi}_n(z_0)e^{-k_n(z-z_0)} \tag{15}$$

and

$$\tilde{E}_{z,n}(z) = k_n\tilde{\Phi}_n(z_0)e^{-k_n(z-z_0)} \tag{16}$$

Consequently, at the bottom interface of such an infinitely thick layer,

$$C_n^*(z_0) = k_n\varepsilon^* \tag{17}$$

The next step is to relate C_n^* at the bottom interface ($z = z_0$) of a layer of thickness t to its value at the upper interface ($z = z_0 + t$). First, consider the Fourier components with $n > 0$. In regions of finite thickness it is more convenient to work with the hyperbolic function equivalent of equation (2):

$$\Phi(x,z) = \cos(kx)\left[b_1'\sinh(kz) + b_2'\cosh(kz)\right] \tag{18}$$

making it possible to express the potential in the layer in terms of its values at the two interfaces as

$$\begin{aligned}\tilde{\Phi}_n(z) = \frac{1}{\sinh(k_n t)}\Big[&\tilde{\Phi}_n(z_0+t)\sinh\left(k_n(z-z_0)\right)\\ &-\tilde{\Phi}_n(z_0)\sinh\left(k_n(z-z_0-t)\right)\Big]\end{aligned} \tag{19}$$

Applying equations (13) and (14) to equation (19) yields the following equations for $C_n^*(z)$ at the two interfaces:

$$\begin{aligned}C_n^*(z_0) &= -k_n\varepsilon^*\left[\frac{\tilde{\Phi}_n(z_0+t)}{\tilde{\Phi}_n(z_0)}\cdot\frac{1}{\sinh(k_n t)} - \coth(k_n t)\right]\\ C_n^*(z_0+t) &= -k_n\varepsilon^*\left[\coth(k_n t) - \frac{\tilde{\Phi}_n(z_0)}{\tilde{\Phi}_n(z_0+t)}\cdot\frac{1}{\sinh(k_n t)}\right]\end{aligned} \tag{20}$$

from which the ratio $\tilde{\Phi}_n(z_0+t)/\tilde{\Phi}_n(z_0)$ can be eliminated to arrive at the following transfer relation:

$$C_n^*(z_0) = k_n\varepsilon^*\frac{C_n^*(z_0+t)\coth(k_n t) + k_n\varepsilon^*}{C_n^*(z_0+t) + k_n\varepsilon^*\coth(k_n t)} \tag{21}$$

To calculate the corresponding transfer relation for $n = 0$, the linear component of equation (2) must be used, leading to:

$$\Phi_0(z) = \frac{(z-z_0)\Phi_0(z_0+t) - (z-z_0-t)\Phi_0(z_0)}{t} \tag{22}$$

and

$$E_{z,0}(z) = -\frac{d}{dz}\Phi_0(z) = -\frac{\Phi_0(z_0+t) - \Phi_0(z_0)}{t} \tag{23}$$

which is, of course, the expression for a uniform electric field between two parallel plane electrodes. At the two interfaces,

$$\begin{aligned}C_0^*(z_0) &= -\frac{\varepsilon^*}{t}\left[\frac{\tilde{\Phi}_0(z_0+t)}{\tilde{\Phi}_0(z_0)} - 1\right]\\ C_0^*(z_0+t) &= -\frac{\varepsilon^*}{t}\left[1 - \frac{\tilde{\Phi}_0(z_0)}{\tilde{\Phi}_0(z_0+t)}\right]\end{aligned} \tag{24}$$

which can be combined to yield the following transfer relation:

$$C_0^*(z_0) = \frac{\varepsilon^* C_0^*(z_0+t)}{tC_0^*(z_0+t) + \varepsilon^*} \tag{25}$$

It may be verified that for an infinitely thick layer, equation (21) approaches equation (17), by taking the limit $t \to \infty$. In this limit, equation (25) approaches

$$C_0^*(z_0) = 0 \tag{26}$$

confirming that leaving out the constant ($n = 0$) Fourier term, as was done in earlier presentations of this model [3], is justified, as long as the top layer is infinitely thick. However, the statement in [3] that "any expression involving C_0^* … can only arise from an externally applied field" is incorrect.

Note also that sensors with cylindrical geometry [8], which use Fourier-Bessel series based on J_0 in place of the Fourier cosine series, do not have the equivalent to this zero-order term. Physically, this is because the cylindrical geometry sensors are limited in extent and thus can have no uniform

electric field component, whereas the Cartesian geometry treated here does assume the sensor to be of infinite extent in the positive and negative *x*- and *y*-directions.

In contrast, in the presence of a top ground plane all Fourier terms make a contribution, including the zero-order term. The surface capacitance density at the bottom interface of the ground-limited top layer can be computed from equations (21) and (25) by taking the limit where $C_n^*(z_0+t)\to\infty$, since $\Phi_n(z_0+t)=0$ at the top interface in contact with the top ground plane:

$$\begin{aligned} C_n^*(z_0) &= k_n\varepsilon^* \coth(k_n t), \qquad n>0 \\ C_0^*(z_0) &= \frac{\varepsilon^*}{t} \end{aligned} \tag{27}$$

which approaches $k_n\varepsilon^*$ for all $n>0$ at sufficiently large values of the thickness *t*, in agreement with the previous results. The $n=0$ terms in equations (25) and (27) are the most significant results in this paper.

At the plane of the electrodes ($z=0$) C_n^* is discontinuous because $\varepsilon^* E_z(x)$ is discontinuous. Using the results obtained so far in this section, it is possible to calculate $C_n^*(z=0^+)$ directly above the electrodes by starting with the layer that is farthest from the sensor, using equations (17) and (26) if it is infinite, and equation (27) otherwise, and then sequentially applying equations (21) and (25) across each layer until the plane of the electrodes is reached.

There is only one layer below the electrodes, the substrate, bounded at the bottom by the substrate ground plane. Using equation (27) and changing the sign of *t* to account for the substrate ground plane position being at $z=-t_S$, we obtain

$$\begin{aligned} C_n^*(z=0^-) &= -k_n\varepsilon_S^* \coth(k_n t_S) \qquad n>0 \\ C_0^*(z=0^-) &= -\frac{\varepsilon_S^*}{t_S} \end{aligned} \tag{28}$$

The quantity σ_S^* is defined as the jump (denoted by double bars) in the normal component of $\varepsilon^*\mathbf{E}$ across an interface:

$$\sigma_S^*(x) = \left\| \varepsilon^* E_z(x) \right\| \tag{29}$$

It would be equal to the surface charge density in the absence of ohmic conduction in the medium. It is zero at every interface except at the electrode surface. Using equation (14), for every Fourier mode, σ_S^* is related to the difference in surface capacitance density above and below the electrodes, $C_n^* \equiv \left\| C_n^*(z) \right\|_{z=0} = C_n^*(0^+) - C_n^*(0^-)$, as

$$\sigma_{Sn}^* = C_n^* \Phi_n, \qquad n=0,1,2,\ldots \tag{30}$$

where σ_{Sn}^* are the coefficients of the Fourier series expansion of $\sigma_S^*(x)$. The jump in the normal component of the total current density can be expressed in terms of $\sigma_S^*(x)$ via equations (11) and (29) as

$$\left\| J_z(x) \right\| = i\omega\sigma_S^*(x) \tag{31}$$

2.4 COLLOCATION POINTS

The geometrical parameters of the IDED are shown in Figure 4, which shows a cross section of half a period of the sensor. In this section we are concerned with the electrostatic potential in the plane of the electrodes, *i.e.*, for $z=0$.

In the gap between the electrodes the electrostatic potential is approximated by an interpolation of its value between a set of $K+2$ collocation points, x_m, $m=0,1,\ldots,K+1$. With the $x=0$ point chosen as shown in Figure 4, symmetry dictates that

$$\Phi(x) = \Phi(-x) \tag{32}$$

which means that only one half of the period needs to be considered in order to determine $\Phi(x)$ uniquely everywhere.

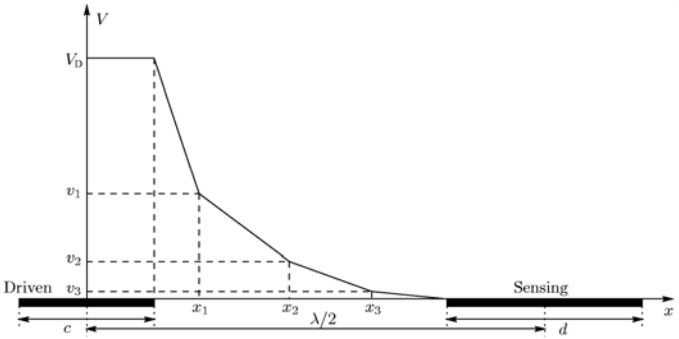

Figure 4. Piecewise-linear collocation-point approximation to the electrostatic potential of the IDED. Three intermediate collocation points at x_1, x_2, and x_3 are shown, *i.e.*, $K=3$ with $x_0=c/2$ and $x_{K+1}=(\lambda-d)/2$. The sensing electrode is shown wider than the driven electrode to emphasize the fact that they do not need to have the same width.

The piecewise-linear representation of $\Phi(x)$ in the gap is given by

$$\begin{aligned} \Phi(x) &= \frac{v_m(x_{m+1}-x)+v_{m+1}(x-x_m)}{x_{m+1}-x_m} \\ x_m &< x < x_{m+1}, \qquad m=0,1,\ldots,K \end{aligned} \tag{33}$$

where v_m are the values of Φ at the points x_m. The first and last collocation points, x_0 and x_{K+1}, are located at the electrode edges, where the potential is known ($v_0=V_D$ and $v_{K+1}=0$). Therefore, there are *K* unknowns that must be determined to find Φ. The collocation points should be concentrated near the edges, where the potential is changing the fastest. One suitable possibility is to follow a simple cosinusoidal distribution:

$$x_m = \frac{c}{2} + \frac{\lambda-c-d}{4}\left[1-\cos\left(\frac{\pi m}{K+1}\right)\right], \qquad 0\le m\le K+1 \tag{34}$$

The value of the potential at the collocation points is determined by integrating the appropriate boundary conditions over a set of *K* intervals, delimited by the points

$x'_\ell, \ell = 0,1,\ldots,K$. Each interval encloses one collocation point. The positions of the interval boundaries are chosen to be half way between the collocation points, except at the two ends:

$$x'_\ell = \begin{cases} x_0 & \ell = 0 \\ (x_{\ell+1} + x_\ell)/2 & \ell = 1,2,\ldots,K-1 \\ x_{K+1} & \ell = K \end{cases} \tag{35}$$

Using equations (5) and (33), it is possible to express the Fourier cosine series coefficients Φ_n for $n > 0$ in the expansion of the potential $\Phi(x)$ in terms of the potential values v_m as follows:

$$\Phi_n = \frac{4}{\lambda}\left[V_\mathrm{D} \int_0^{x_0} \cos(k_n x)\,dx + \sum_{m=0}^{K} \int_{x_m}^{x_{m+1}} \cos(k_n x) \frac{v_m (x_{m+1} - x) + v_{m+1}(x - x_m)}{x_{m+1} - x_m} dx \right], \quad n > 0 \tag{36}$$

The first term in equation (36) results from integration over the driven electrode, where the potential is constrained to be equal to the driving voltage V_D. The potential is zero at the sensing electrode and therefore this interval does not contribute to the integral. Carrying out the integration yields

$$\Phi_n = \frac{4}{\lambda k_n}\left\{ V_\mathrm{D} \sin(k_n x_0) + \sum_{m=0}^{K} \frac{v_{m+1} - v_m}{x_{m+1} - x_m} \left[\cos(k_n x_{m+1}) - \cos(k_n x_m) \right] + \sum_{m=0}^{K} \left[v_{m+1} \sin(k_n x_{m+1}) - v_m \sin(k_n x_m) \right] \right\}, \quad n > 0 \tag{37}$$

The terms in the second summation in equation (37) cancel each other on a term-by-term basis, except for the two end terms multiplying $v_0 = V_\mathrm{D}$ and $v_{K+1} = 0$. The latter is at the sensing electrode edge, where the potential is zero and can be ignored. This results in

$$\Phi_n = -\frac{4}{\lambda k_n^2}\left\{ \sum_{m=1}^{K} v_m \left[\frac{\cos(k_n x_{m+1}) - \cos(k_n x_m)}{x_{m+1} - x_m} - \frac{\cos(k_n x_m) - \cos(k_n x_{m-1})}{x_m - x_{m-1}} \right] + V_\mathrm{D} \frac{\cos(k_n x_1) - \cos(k_n x_0)}{x_1 - x_0} \right\}, \quad n > 0 \tag{38}$$

where the coefficients multiplying v_m have been consolidated. Note that in equation (38), the index of the summation starts at $m = 1$. The $m = 0$ term has been written out separately, because $v_0 = V_\mathrm{D}$ is known.

The $n = 0$ constant term in the Fourier expansion may similarly be evaluated via equations (6) and (33) as

$$\begin{aligned} \Phi_0 &= \frac{2}{\lambda}\left[\int_0^{x_0} V_\mathrm{D}\,dx + \sum_{m=0}^{K} \int_{x_m}^{x_{m+1}} \frac{v_m (x_{m+1} - x) + v_{m+1}(x - x_m)}{x_{m+1} - x_m} dx \right] \\ &= \frac{1}{\lambda}\left[2V_\mathrm{D} x_0 + 2\sum_{m=0}^{K} (v_m x_{m+1} - v_{m+1} x_m) + \sum_{m=0}^{K} (v_{m+1} - v_m)(x_{m+1} + x_m) \right] \\ &= \frac{1}{\lambda}\left[V_\mathrm{D}(x_0 + x_1) + \sum_{m=1}^{K} v_m (x_{m+1} - x_{m-1}) \right] \end{aligned} \tag{39}$$

2.5 BOUNDARY CONDITIONS

The relevant boundary condition in the gap between electrodes is

$$\sigma_\mathbf{S}^*(x) = 0 \tag{40}$$

which results from equation (31), since there is no electrode to act as a current source or sink, and no surface conduction is considered. If surface conductivity and permittivity are present, they may be incorporated in the model by introducing an additional material layer and taking the limit as its thickness approaches zero. The integral of the condition in equation (40), over every interval $x'_\ell < x < x'_{\ell+1}$, where x'_ℓ is defined in equation (35), is

$$\begin{aligned} &\int_{x'_\ell}^{x'_{\ell+1}} \sigma_\mathrm{S}^*(x)\,dx \\ &= \sum_{n=1}^{\infty} \int_{x'_\ell}^{x'_{\ell+1}} C_n^* \Phi_n \cos(k_n x)\,dx + \int_{x'_\ell}^{x'_{\ell+1}} C_0^* \Phi_0\,dx \\ &= \sum_{n=1}^{\infty} C_n^* \Phi_n \frac{1}{k_n}\left[\sin(k_n x'_{\ell+1}) - \sin(k_n x'_\ell) \right] + C_0^* \Phi_0 \left(x'_{\ell+1} - x'_\ell \right) \\ &= \sum_{n=0}^{\infty} C_n^* \sum_{m=1}^{K} M_{\ell,m}^n v_m - \sum_{n=0}^{\infty} C_n^* b_\ell^n = 0 \end{aligned} \tag{41}$$

The last relation in equation (41) comes from substituting equations (38) and (39) into the equation and grouping together the terms multiplying v_m into the coefficient matrices $\mathbf{M}^n$ with elements $M_{\ell,m}^n$, and elements independent of v_m into vector $\mathbf{b}^n$ with elements b_ℓ^n.

One equation results from the application of the boundary condition over each of the integration intervals. In matrix form this set of equations can be written as

$$\mathbf{M}\mathbf{v} = V_\mathrm{D}\mathbf{b} \tag{42}$$

where $\mathbf{v}$ is a vector of the unknown potential values v_m. The matrix $\mathbf{M}$ can be derived from equation (41):

$$\mathbf{M} = \sum_{n=0}^{\infty} C_n^* \mathbf{M}^n \tag{43}$$

The advantage of formulating **M** as a summation of the sub-matrices $\mathbf{M}^n$ is that the sub-matrices depend only on the sensor parameters, and need to be computed once when calculating the sensor response for a variety of material properties and geometries, where each configuration has a different set of C_n^* values. After substituting equations (38) and (39) into equation (41), the elements of $\mathbf{M}^n$ are determined to be:

$$M_{\ell,m}^n = -\frac{4}{\lambda k_n^3}\left[\sin(k_n x'_{\ell+1}) - \sin(k_n x'_\ell)\right] \times \times \left[\frac{\cos(k_n x_{m+1}) - \cos(k_n x_m)}{x_{m+1} - x_m} - \frac{\cos(k_n x_m) - \cos(k_n x_{m-1})}{x_m - x_{m-1}}\right], \quad n > 0 \tag{44}$$

and

$$M_{\ell,m}^0 = \frac{1}{\lambda}\left(x'_{\ell+1} - x'_\ell\right)\left(x_{m+1} - x_{m-1}\right) \tag{45}$$

The right hand side vector **b** of the matrix equation (42) can similarly be expressed as a summation over Fourier modes:

$$\mathbf{b} = \sum_{n=0}^{\infty} C_n^* \mathbf{b}^n \tag{46}$$

Extracting the constant terms from equations (38) and (39) gives for the ℓ th element of the vector $\mathbf{b}^n$

$$\mathbf{b}_\ell^n = \frac{4}{\lambda k_n^3}\left[\sin(k_n x'_{\ell+1}) - \sin(k_n x'_\ell)\right]\frac{\cos(k_n x_1) - \cos(k_n x_0)}{x_1 - x_0}, \quad n > 0 \tag{47}$$

and

$$\mathbf{b}_\ell^0 = -\frac{1}{\lambda}\left(x'_{\ell+1} - x'_\ell\right)\left(x_0 + x_1\right) \tag{48}$$

Solving the matrix equation results in full knowledge of the electrostatic potential $\Phi(x)$ at the plane of the electrodes.

2.6 CALCULATING TRANSCAPACITANCE

The transcapacitance is related to the transadmittance via

$$C_\mathrm{T} = \frac{Y_{21}}{i\omega} = \frac{I_\mathrm{S}}{i\omega V_\mathrm{D}} \tag{49}$$

It is obtained by calculating the terminal current I_S in equation (49). The terminal current out of the sensing electrode is equal to the negative of integral over the sensing electrode area of the jump in the normal component of the total current density:

$$I_\mathrm{S} = -\int_{x_{K+1}}^{\lambda/2} \left\| J_z(x) \right\| dx \tag{50}$$

Using equations (30), (31), (49), and (50), an expression for the transcapacitance can be obtained:

$$C_\mathrm{T} = -\frac{L}{V_\mathrm{D}}\left[\sum_{n=1}^{\infty}\int_{x_{K+1}}^{\lambda/2} C_n^* \Phi_n \cos(k_n x)\, dx + \int_{x_{K+1}}^{\lambda/2} C_0^* \Phi_0\, dx\right] \tag{51}$$

where L is the meander length of the sensor, *i.e.*, the finger length in the y-direction multiplied by the number of fingers of the sensing electrode.

In order to express the transcapacitance C_T in terms of the vector of potential values v_m calculated by solving the matrix equation (42), equations (38) and (39) are substituted into equation (51), yielding

$$C_\mathrm{T} = -L\sum_{n=1}^{\infty} C_n^* \sin(k_n x_{K+1}) \frac{4}{\lambda k_n^3}\left\{\frac{\cos(k_n x_1) - \cos(k_n x_0)}{x_1 - x_0} + \right. + \sum_{m=1}^{K}\frac{v_m}{V_\mathrm{D}}\left[\frac{\cos(k_n x_{m+1}) - \cos(k_n x_m)}{x_{m+1} - x_m} - \frac{\cos(k_n x_m) - \cos(k_n x_{m-1})}{x_m - x_{m-1}}\right]\Bigg\} - \frac{L}{\lambda} C_0^*\left(\frac{\lambda}{2} - x_{K+1}\right)\left[x_0 + x_1 + \sum_{m=1}^{K}\frac{v_m}{V_\mathrm{D}}(x_{m+1} - x_{m-1})\right] \tag{52}$$

where the sensing electrode extends from $x_{K+1} = \lambda/2 - d/2$ to $\lambda/2$.

3 MODEL APPLICATION AND EXPERIMENTAL RESULTS

To illustrate the validity of the model, it was applied to the IDED in Figure 5, and a number of measurements were made with this sensor. The sensor was manufactured on a $t_\mathrm{S} = 0.508$ mm thick Teflon substrate with permittivity $\varepsilon_\mathrm{S} = 2.1\varepsilon_0$, where ε_0 is the permittivity of vacuum. Teflon was the material of choice for the substrate, because its low dielectric constant, one of the lowest among solids, optimizes sensitivity to the material structure above the sensor; and because its hydrophobic properties make it less susceptible to ambient humidity levels and to contamination. The spatial wavelength of the sensor was $\lambda = 2$ mm. The sensing electrode had five 20-mm long fingers, for a total meander length of $L = 100$ mm. In order to eliminate edge effects, two grounded guard fingers were present on either side of the active area. All measurements were carried out at 39.8 kHz. With this spatial wavelength, the characteristic Laplacian decay length of the fundamental Fourier mode is $\lambda/2\pi \approx 0.32$ mm; therefore it should be expected that the sensor will be relatively insensitive to the properties of materials further than about 0.5 mm from the sensor surface.

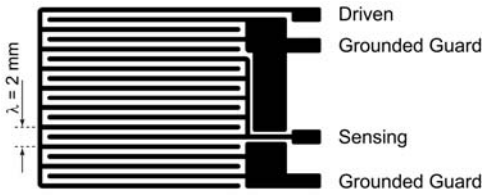

Figure 5. IDED with $\lambda = 2$ mm, $t_\mathrm{S} = 0.508$ mm, $\varepsilon_\mathrm{S} = 2.1\varepsilon_0$, and $L = 0.1$ m.

In the absence of material conductivity, the sensor transcapacitance has no imaginary component, because

when $\sigma = 0$, ε^* is real in all material layers. More precisely, at this operating frequency for the materials used, $\sigma/\omega \ll \varepsilon$, such that any imaginary component of the transcapacitance C_T would be overcome by instrumentation noise. Therefore, in a measurement with this sensor, only one unknown property of the material structure may be independently estimated, typically a dielectric layer permittivity or thickness. The sensor response is most strongly influenced by the properties of the closest material layer. Unless the sensor is immersed in a liquid [4, 5], this is an air layer, whose thickness is also known as the *lift-off*. The sensor lift-off is always present, because the electrodes have a finite nonzero thickness, and because it is in general difficult to create perfectly flat sensors and specimens, and to eliminate all intervening dust particles. Thus the sensor's transcapacitance is most sensitive to the lift-off. At the same time, the lift-off is very difficult to control and to measure independently by other means, because the effective lift-off due to the electrode thickness is unknown, and because material layers with thicknesses on the order of a fraction of a millimeter do not maintain their rigidity well enough over the area of the sensor.

These considerations lead to the conclusion that it is difficult to design an experiment that uses only a single-wavelength sensor. For these reasons a lot of research has focused on the development of multiple-wavelength sensors, especially those that have more than one effective wavelength within the same sensor footprint, which allows for independent estimation of multiple unknowns [8, 6]. Nonetheless, we were successful in designing two experiments, one with and one without a top ground plane, where the relative significance of the lift-off was minimized by measuring on a low dielectric constant material, Teflon, with $\varepsilon = 2.1\varepsilon_0$, and placing above it a material with contrasting dielectric properties, a thick layer of glass with $\varepsilon = 7.8\varepsilon_0$ in the former case, and a grounded top plane in the latter. The setup for these two experiments is shown in Figure 6.

In both cases, the estimated parameter was the layer thickness t_2, which is much easier to control than the lift-off. In computing the sensor response, the lift-off was kept constant at $t_1 = 21.5$ μm. This value was estimated from a preliminary dielectrometry measurement, where a thick Teflon block was placed directly on top of the sensor, in a setup similar to that in Figure 6(a), with no glass and with an infinitely thick Teflon layer. In that measurement the lift-off was the only unknown parameter. To make sure the lift-off was the same in that and all subsequent measurements, the pressure in the material structure was kept constant via a 2.5 kg weight. In the case without a top ground plane, the top dielectric layer was thick enough so that the presence of the weight had no effect on the electric field. From this point on, all calculated sensor responses incorporated a lift-off layer with this thickness.

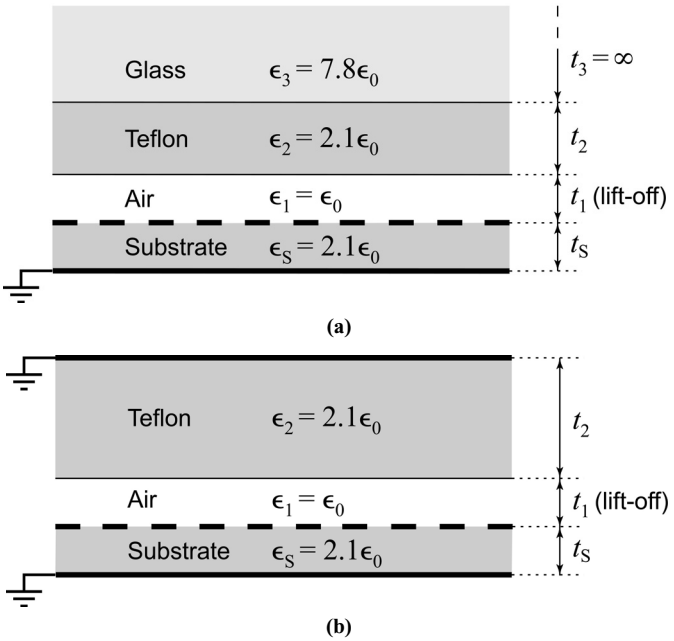

Figure 6. Experimental setup for measuring a dielectric layer's thickness: (a) topped by a thick dielectric slab of known permittivity, and (b) topped by a grounded metal plane.

The Teflon layer thickness was varied by stacking up one through seven sheets, each with an approximate thickness of 75 μm (0.003 in.). Figure 7 shows a family of curves with different values for ε_2, obtained with the model described in the previous section, that relate the sensor transcapacitance C_T to the dielectric thickness t_2, for the setup in Figure 6(a). In agreement with the earlier rough estimate of the depth of sensitivity, it is clear from the figure that the measurement becomes insensitive to the thickness above about 0.5 mm, indicating that the measurement uncertainty would be too great if more than about seven sheets are used. The results from the measurements are also plotted in Figure 7 and listed in Table 1. It can be seen that the estimated thickness follows the nominal thickness well, bearing in mind the uncertainty introduced by the fixed lift-off assumption and by the presence of air gaps between the individual Teflon sheets, and the fact that the sensor becomes increasingly insensitive as the thickness approaches the limit of the depth of sensitivity.

Table 1. Results from single-unknown Teflon thickness t_2 estimation for the two setups with and without a grounded top plane.

Number of Teflon sheets	Nominal thickness t_2 [μm]	Estimated thickness without a top ground plane [μm]	Estimated thickness with a top ground plane [μm]
1	75	85	80
2	150	151	160
3	225	236	236
4	300	310	320
5	375	373	395
6	450	458	495
7	525	549	585

It should be noted that in Figure 7 the magnitude of the signal changes monotonically with thickness. For $\varepsilon_2 = \varepsilon_3 = 7.8\varepsilon_0$ the curve is flat, since the two layers cannot

be distinguished, and all values of t_2 yield the same response. When $\varepsilon_2 < \varepsilon_3$ the curves decrease monotonically and for $\varepsilon_2 > \varepsilon_3$ the curves increase monotonically.

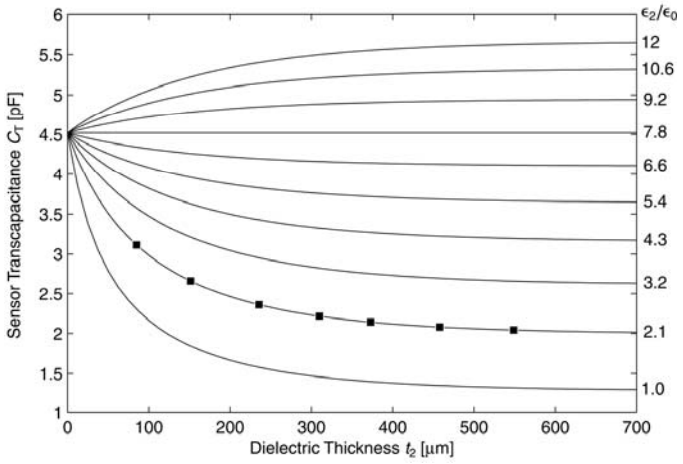

Figure 7. Family of curves and experimental results for the case without a top ground plane. The calculated and measured sensor transcapacitance is plotted as a function of t_2 in Figure 6(a), for a range of permittivities of that layer.

The same data used to generate the curves in Figure 7 was used to plot the calculated sensor transcapacitance as a function of permittivity in Figure 8. It is clear from this figure that in the absence of a top ground plane, a permittivity measurement is always unique, because no two values produce the same value for the sensor transcapacitance. The figure also illustrates the loss of sensitivity to layer thicknesses greater than 500 μm, seeing how close the $t_2 = 500$ μm curve is to the $t_2 = \infty$ curve. As discussed earlier, for $\varepsilon_2 = \varepsilon_3 = 7.8\varepsilon_0$ the transcapacitance is independent of the thickness, and consequently all curves in Figure 8 must pass through the same point.

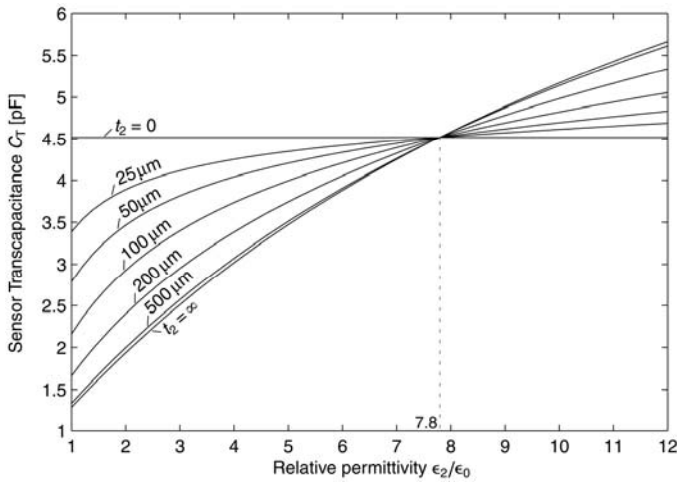

Figure 8. Family of calculated curves for the case without a top ground plane. The sensor transcapacitance is plotted as a function of ε_2 in (b)(a), for a variety of thicknesses of that layer.

Now consider the experimental setup in Figure 6(b). The analogous family of curves and data points for this case are shown in Figure 9. The results of the measurements are also listed in Table 1. The reason the measured thickness tends to be overestimated are the air gaps between the individual Teflon sheets. The sensor transcapacitance is generally lower in the case with a top ground plane, because of its shielding effect, whereby some of the field lines, which would otherwise have terminated on the sensing electrode, now terminate on the grounded top plane. There are several interesting features evident in this figure.

For thicknesses greater than about 340 μm, the transcapacitance increases with dielectric permittivity, because in this case the top ground plane is far enough away so that the effect of the dielectric dominates. However, for low values of the thickness, increasing the permittivity leads to lower values of the transcapacitance because the dielectric acts to steer some of the field lines away from the sensing electrode and toward the top ground plane, thus increasing its shielding effect. Near the critical thickness of about 340 μm it is not clear from the plot in Figure 9 how the transcapacitance varies with permittivity, other than to say that it is quite insensitive to it. Note that although any two curves in the figure do cross, the intersection points do not coincide, as can be seen in the inset in the figure.

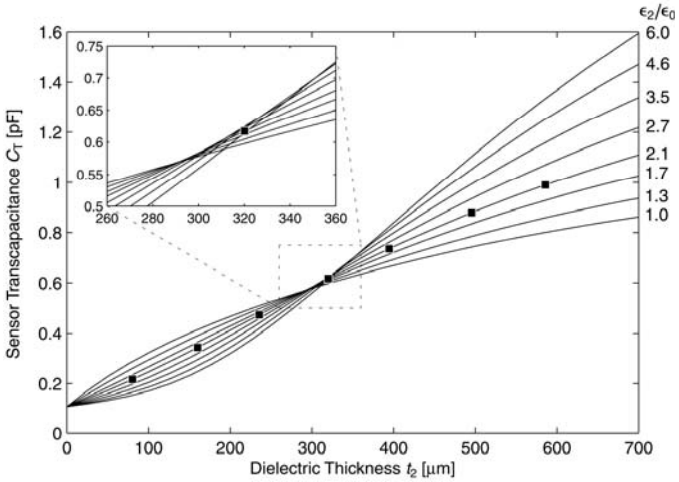

Figure 9. Family of calculated curves and experimental results for the case with a top ground plane. The sensor transcapacitance is plotted as a function of t_2 in Figure 6(b), for a range of permittivities of that layer.

In order to investigate how the sensor signal depends on permittivity near this critical thickness, the transcapacitance is plotted as a function of the dielectric permittivity for a closely spaced set of thicknesses in Figure 10. For thicknesses less than ~300 μm the magnitude is monotonically decreasing, a result also evident in Figure 9. Though not obvious from the data in Figure 10, which does not show the behavior for very large values of the permittivity, it is certain that there is a thickness beyond which the magnitude is monotonically increasing, because in the limit of infinite thickness the configuration without a top ground plane must be approached. However, there is a range of thicknesses where a permittivity measurement would be double-valued, in contrast with the

case that does not incorporate a top ground plane. For example, consider the task of measuring the permittivity of a 310-μm-thick dielectric layer, with transcapacitance measured to be 0.597 pF. The answer can be obtained graphically as the intersection of the dashed line in Figure 10 with the 310-μm curve. There are two possible solutions: $\varepsilon_2 = 1.7\varepsilon_0$ and $\varepsilon_2 = 4.6\varepsilon_0$.

Note that although it is thus possible for a permittivity measurement to be nonunique, a thickness measurement with known permittivity poses no such difficulties, as illustrated by the set of measurement results in Figure 9.

Another feature to note in Figure 9 is that the curves do not flatten out beyond 500 μm as in Figure 7, indicating that the presence of the top ground plane increases the depth of sensitivity. This is because in this case the electric fields are no longer dominated by the fundamental cosinusoidal Fourier mode $n = 1$. The presence of a nonzero uniform field component (the $n = 0$ mode) means that the electric field no longer decays exponentially, but retains a constant component, making the sensor sensitive to material properties throughout the entire material structure.

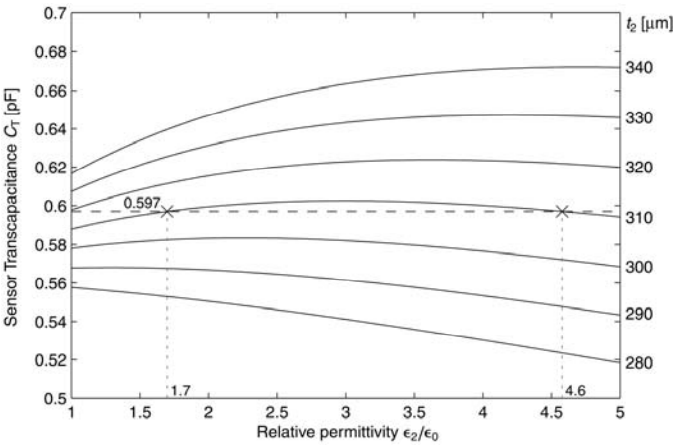

Figure 10. Calculated sensor transcapacitance as a function of permittivity in the presence of a top ground plane, for various dielectric thicknesses t_2 in the vicinity of the critical thickness (~300 μm). The dashed line illustrates how a permittivity measurement may be double-valued.

4 SUMMARY

In this paper we have extended the collocation point model, used for predicting the response of interdigitated dielectrometers, to treat the presence of a grounded top plane bounding the dielectric layer structure. This makes it possible to carry out measurements with a grounded metal plane present, which can improve measurement repeatability by eliminating the effects of conducting or dielectric objects in the vicinity of the sensor. Furthermore, it enables measurements in cases where such a metal plane is an integral part of the structure, such as ceramic thermal barrier coatings.

It has been shown that the presence of the top ground plane has profound implications, not just quantitative, but also qualitative. For example, it can make a sensor insensitive to the permittivity of the material, or make it yield nonunique results. The validity of the model has been confirmed by a set of measurements with a single-wavelength IDED, both with and without the presence of a grounded top plane.

REFERENCES

[1] A. Washabaugh, Y. Sheiretov, D. E. Schlicker and N. J. Goldfine, "Non-Contact Capacitive Sensing Dielectrometers for Characterization of Adhesives and Epoxies", ASNT Fall Conf., Indianapolis, IN, USA, pp. 155-157, 2000.

[2] N. J. Goldfine, T. Lovett, Y. Sheiretov and P. J. Zombo, "Dielectrometers and Magnetometers, Suitable for In-situ Inspection of Ceramic and Metallic Coated Components", SPIE Proc., Vol. 2459, pp. 164–174, 1995.

[3] M. C. Zaretsky, L. Mouayad and J. R. Melcher, "Continuum Properties from Interdigital Electrode Dielectrometry", IEEE Trans. Electr. Insul., Vol. 23, pp. 897–917, 1988.

[4] Y. Sheiretov, *Dielectrometry Measurements of Moisture Dynamics in Oil-Impregnated Pressboard*, M.S. thesis, Department of Electrical Engineering and Computer Science, Massachusetts Institute of Technology, Cambridge, MA, May 1994.

[5] Y. Sheiretov and M. Zahn, "Dielectrometry Measurements of Moisture Dynamics in Oil-Impregnated Pressboard", IEEE Trans. Dielectr. Electr. Insul., Vol. 2, pp. 329–351, 1995.

[6] Y. Sheiretov, *Deep Penetration Magnetoquasistatic Sensors*, Ph.D. thesis, Department of Electrical Engineering and Computer Science, Massachusetts Institute of Technology, pp. 48–59, 69–75, 2001.

[7] F. B. Hildebrand, *Advanced Calculus for Applications*, 2nd Edition, Prentice-Hall, Inc., Englewood Cliffs, NJ, 1976.

[8] I. Shay (Y. Sheiretov) and M. Zahn, "Cylindrical Geometry Electroquasistatic Dielectrometry Sensors," IEEE Trans. Dielectr. Electr. Insul., Vol. 12, pp. 41–49, 2005.

Yanko Sheiretov (has also published under the name Ian C. Shay) was born in Sofia, Bulgaria in 1970. He holds the position of Senior Scientist and Lead Software Architect at JENTEK Sensors, Inc. in Waltham, MA, USA. Dr. Sheiretov recently completed the requirements for the Ph.D. degree in electrical engineering at MIT. His doctoral thesis, entitled "Deep penetration magnetoquasistatic sensors", describes research on integration of a GMR sensor with a circular, periodic drive winding. Dr. Sheiretov also has experience in several areas of electrical and computer engineering and applied physics, including electromagnetic field and sensor analysis and modeling; solid state infrared laser design, testing and microfabrication; power electronics; wireless telecommunications; analog and digital system design. His software development experience has focused on numerical methods, data modeling and analysis, robust numerical estimation on a variety of platforms, including C++, Fortran, Basic, Common Lisp, and data analysis packages such as MATLAB, Maple, and Mathematica. He also has experience in GUI software design for Windows, UNIX/X and Macintosh platforms. Dr. Sheiretov obtained the BS, MS, EE, and Ph.D. degrees in 1992, 1994, 1998 and 2001, respectively from the Massachusetts Institute of Technology. He is a recipient of the 1992 Henry Ford II Scholar Award for Academic Excellence and member of Eta Kappa Nu honor society.

Markus Zahn (F'93) is the Thomas and Gerd Perkins Professor of Electrical Engineering at MIT. He was born in Bergen-Belsen, Germany in 1946. He received the BSEE and MSEE degrees in 1968, the Electrical Engineers degree in 1969, and the Sc.D. degree in 1970, all from the Department of Electrical Engineering at the Massachusetts Institute of Technology. From 1970-1980 he was a Professor of Electrical Engineering at the University of Florida,

Gainesville. He joined the MIT faculty in 1980 and works in the Laboratory for Electromagnetic and Electronic Systems and in the MIT High Voltage Research Laboratory. He is also the Director of the MIT Course VI-A Electrical Engineering and Computer Science Internship Program, a cooperative work/study program with Industry.

Since 1992 he has had numerous visiting appointments in France, Japan, and Israel (Technion) university and research centers. He was a Paris, France Sciences Scholar for 2000 and received the Ecole Superieure de Physique et de Chimie Industrielle (ESPCI) medal.

He is the author of Electromagnetic Field Theory: A Problem Solving Approach (Wiley, 1979; Krieger, 1987, 2003; including translations in Spanish and Polish) and has co-developed a set of educational videotapes on Demonstrations of Electromagnetic Fields and Energy. He is co-inventor on 13 patents plus four more patents pending.

Professor Zahn has received numerous awards for excellence in teaching, including the MIT Graduate Student Council Teaching Award in 1989 and the MIT Frank E. Perkins award for excellence in graduate student advising in 1999. He is serving as Associate Editor of the Transactions on DEI, Chairman of the Liquid Dielectrics Committee, and is on the International Advisory Committee of the International Conference on Dielectric Liquids.

He was the 1998 J.B. Whitehead Memorial Lecturer of the IEEE Conference on Electrical Insulation and Dielectric Phenomena. He was also the First James R. Melcher Memorial Lecturer at the First Joint Meeting of the IEEE Industry Applications Society-Electrostatic Processes Committee and the Electrostatic Society of America, Little Rock, AR in 2003. He serves on the Academic Advisory Board of the W.M. Keck Laboratory for Electro-Hydrodynamics of Suspensions at the New Jersey Institute of Technology and was a member of the National Academies Naval Studies Board Committee for Mine Warfare Assessment.